Synthesis, evaluation, and monitoring of red amaranth extract for power production

Article *in* Advances in Natural Sciences Nanoscience and Nanotechnology · January 2024

DOI: 10.1088/2043-6262/ad1a9f

3 authors, including:

Nilufer Yesmin Tanisa
Uttara University
15 PUBLICATIONS **29** CITATIONS

SEE PROFILE

IOP Publishing | Vietnam Academy of Science and Technology Advances in Natural Sciences: Nanoscience and Nanotechnology

Adv. Nat. Sci.: Nanosci. Nanotechnol. **15** (2024) 015001 (9pp) https://doi.org/10.1088/2043-6262/ad1a9f

Synthesis, evaluation, and monitoring of red amaranth extract for power production

N Y Tanisa[1,2], K A Khan[3] and M Salahuddin[2]

[1] Department of Physics, Uttara University, Dhaka-1230, Bangladesh
[2] Department of Physics, Jahangirnagar University, Dhaka-1342, Bangladesh
[3] Department of Physics, Jagannath University, Dhaka-1100, Bangladesh

E-mail: tanisha.90@uttarauniversity.edu.bd

Received 11 April 2023
Accepted for publication 18 October 2023
Published 16 January 2024

Abstract

The scientific paper describes the synthesis of silver nanoparticles (Ag NPs) using a fresh red amaranth preparation and explores their potential to enhance the output current of a red amaranth bio-electrolytic cell. The study employed various analytical techniques such as x-ray diffraction (XRD), Fourier transform infrared (FTIR), ultraviolet-visible spectroscopy (UV–vis), dynamic light scattering (DLS), and Raman spectroscopy to characterise and detect the nanoparticles. The UV–vis analysis of the dripping media containing silver nanoparticles exhibited an absorption peak, indicating the presence of the nanoparticles. FTIR was utilised to examine the interaction between the biomaterial components and the oxidation and wrapping of silver nanoparticles. XRD analysis revealed that the synthesised nanoparticles possessed a naturally columnar shape and a face-centered cubic (FCC) structure. The average size and morphology of the nanoparticles were characterised by dynamic light scattering (DLS). Raman spectra revealed the unique surface-enhancing properties of synthesised Ag NPs. The research presented in the paper highlights the remarkable performance of silver nanoparticles in bio-electrolyte power generation systems. It emphasises a straightforward, cost-effective, and environmentally friendly method for producing Ag NPs using red amaranth extract. These findings contribute to the development of a novel framework for bio-electrochemical cells and emphasise the importance of further research on the effects of Ag NPs on these cells. It is found that the open circuit voltage is 3.254 V, short circuit current is 2.256 mA, and load current is 1.987 mA before using the Ag NPs and open circuit voltage is 5.678 volts, short circuit current is 4.212 mA, and load current is 2.887 mA after using the Ag NPs. It is seen that the values of the three parameters have been increased after using the Ag NPs, which ensured the significance of the use of Ag NPs.

Keywords: UV-visible, DLS, XRD, power monitoring, Raman analysis, Ag NPs, FTIR
Classification numbers: 2.00, 2.01, 4.00, 4.04, 5.00

1. Introduction

Nanotechnology is one of the most active study fields in modern materials science. Materials and structures with diameters ranging from 1 to 100 nm are often used. According to recent investigations [1–3], extracts from fungi, bacteria, and plants can be used to make silver nanoparticles (Ag NPs). Nanoscale materials are used in physics, chemistry, biology, material science, agriculture, and medicine because of their unique optical, thermal, electric, and/or magnetic properties. Appropriate nanoscience is employed in research and technology to solve difficulties in a wide range of sectors, including medicine, catalysis, mechanical work, and agriculture [4, 5]. Especially, for the past few years, much effort has been made to develop novel methods to prepare nanostructured metal chalcogenide semiconductors [6]. Extracts from *Amaranthus* species may have antibacterial properties, according to certain studies. In previous research, *Alternaria alternate*, *Fusarium solani*, *Candida albicans*, *Fusarium oxysporum*, *Trichoderma* sp., and *Aspergillus ochraceus* growth was found to be considerably inhibited by *A. hypochondriacs* protein extract [7].

In our investigation, we extracted Ag NPs from the leaves of Chinese red spinach (*Amaranthus gangeticus* Linn).

It is a native shrub that grows abundantly in our environment and is mostly used as a food source. Various flame retardant additives, such as halogenated compounds, are limited with respect to environmental requirements [8, 9]. A new catalytic method was developed for the selective benzylation of benzene to diphenylmethane using alumina-supported metal chloride ($FeCl_3$, $MnCl_2$, $CoCl_2$, $NiCl_2$, $CuCl_2$, and $ZnCl_2$) as the catalyst and benzyl chloride as the benzylating agent. Metals and metal oxide nanoparticles (NPs) have magnetic, electrical, and catalytic antibacterial activities due to their wide surface area and high atom concentration [10–15]. The synthesis and characterisation of copper (II) complexes of 14-membered hexaaza macrocycles were reported [16]. The synthesis and characterisation of transition metal (Mn (II), Co (II), Ni (II) and Cu (II)) complexes of the Schiff-base ligand were studied. The Amaranthaceae family includes the herbaceous plant *Amaranthus caudatus* Linn (*A. caudatus* L.), also referred to as amaranth. It is a green, palatable vegetable known in Yoruba as 'Efotete' [17]. It cleans the blood and is used to treat kidney disease and jaundice. It contains antioxidant, anti-atherosclerotic, anti-helminthic, anti-microbial, anti-cancer, anti-inflammatory, anti-diabetic, and antipyretic properties because of its high polyphenolic content [18–20]. α-Fe_2O_3 nanoparticles were synthesised using *T. aurea* leaf extract and characterised using various techniques [18]. Historically, silver has been used as a conductive wire in circuits that need low dissipation and high conductivity [21–24]. Reported photocatalytic and electrocatalytic ternary systems of $Fe_2O_3/EuVO_4/g\text{-}C_3N_4$ nanocomposites were synthesised through a son chemical procedure. Also, the photocatalytic activity of nanostructures and hybrid nanocomposites was investigated using cationic Rhodamine B dye under visible source irradiation [24].

Currently, $TmVO_4/Fe_2O_3$ nanocomposites were successfully prepared through a simple, fast, and low-cost sonochemical approach for the first time [25, 26]. The results regarding MnO_2 nanoparticles, produced from PKL extract as a reducing agent, have been used to generate electricity for practical utilisations. The Ag NPs were applied on the bio-voltaic cell to examine the electrical performances of the cell [27, 28]. It has been published in several papers using different kinds of extract-based bio-electrochemical cells [27, 28]. The fundamental distinction among those papers is decreasing the internal resistance (V_{oc}/I_{oc}).

We demonstrate how red amaranth leaf extract and silver nitrate solution were used to create silver nanoparticles in an aqueous solution. It has been demonstrated that red amaranth leaf extract has the capacity to produce silver nanoparticles. In this work, the power development of red amaranth extract-based Zn/Cu electrochemical cells employing Ag NPs has been explored.

2. Resources and techniques

2.1. Preparation of plant material

A 20-gram piece of clean red amaranth was purchased from the market, carefully cleaned with distilled water, and then repeatedly sanitised with de-ionised solutions. The red amaranth was then crushed and rinsed until it was mush. After that, 100 ml of de-ionised water was added to the red amaranth mixture, which was then heated to 62 °C for 60 min while continuously spinning on a magnetic field. The extract mixture was chilled. To eliminate any remaining particles, the mixture is filtered through two Whatman 41 and Whatman 42 filters after cooling. Then, the red amaranth leaf solution was kept in a freezer set at 5 °C for further use.

2.2. Development of silver nanoparticles

Sigma Aldrich supplied a very pure $AgNO_3$ chemical for this study. 45 ml of a reaction mixture ($AgNO_3$) at 1.0 mM was put into a 100 ml conical flask. After that, 5 ml of red amaranth extract was gently blended in. After a gentle shake, the mixture was placed in the eclipse for two hours, during that time it changed colour from yellow to maroon. The formation of Ag NPs is confirmed after a few days when the solution turns black with some black sediment at the bottom of the flask. The method flow for producing Ag nanoparticles from red amaranth extract is depicted in figures 1, and 2 depicts the visual alterations that occur as Ag NPs form.

2.3. The essential concept of a synopsis cell

A zinc/copper-red amaranth biological cell was built by using zinc and copper sheets as electrodes, red amaranth fluid as an electrolyte, and environmentally generated silver nanoparticles as a reaction. Electrons are picked up by the Cu board, moved to the Zn sheet, and then interact with the hydrogen ion and Cu^{2+} ions in this system. These ions are slowly transformed into H_2 and copper atoms. Cells have been emitting H_2 gas for a long time, and Cu atoms have been added to the copper sheet.

2.4. Designing nanoparticle cell structures

Three unique organic cells were built to investigate how silver nanoparticles impact energy generation processes. In case 1, zinc and copper sheets were used as conductors, with identical bottom portions on both conductors. 100 ml of red amaranth extract and 5 ml of $AgNO_3$ combination were used as cell electrolytes. The cell liquid solution was then treated with a 20 ml dose of an Ag NPs combination. In case 2, zinc and copper plates were used as conductors. In case 3, the electrolytes were 100 ml of red amaranth solution. The architecture of three organic cells is seen in figure 3.

2.5. Ag NPs energy-generating activities

Throughout cases 1, 2, and 3, the voltage in the open circuit and current in the short circuit were noted. To use the method,

Figure 1. Steps: (a) Fresh red amaranth, (b) Mixing red amaranth in a blender, (c) Mashed red amaranth, (d) Mashed red amaranth with de-ionised water, (e) Heating at 62 °C for 60 min with a magnetic stirrer with a hot plate, (f) Filtrating red amaranth extract with Whatman paper, (g) $AgNO_3$ and filtered red amaranth extract, (h) Ag NPs are synthesised using red amaranth extract, and (i) The powder form of Ag NPs), as shown in the diagram.

the energy of different cells was estimated as

$$P = V_{oc} \times I_{sc}$$

and the formula to calculate the cells' resistance is

$$R_{\text{in}} = V_{oc}/I_{sc}$$

here, P = the cell's power, R_{in} = the cell's inner resistance, V_{oc} = the cell's voltage in the open circuit, I_{sc} = the cell's current in the short circuit.

2.6. Biosynthesised Ag NPs properties

The crystal structure is evaluated using x-ray diffractometer (XRD) technology. Both the produced nanoparticles and the red amaranth extract were examined for the presence of functional groups using the Fourier transform infrared (FTIR) method. An aqueous medium containing silver nanoparticles has an absorption peak that was measured using UV–visible spectroscopy. Using an ultraviolet-visible spectrophotometer, the green produced Ag NPs were examined, and the spectra of the reaction mixture were determined in the vicinity (250 nm –700 nm). The Rigaku x-ray generation system was used to examine the crystalline condition of silver nanoparticles. X-ray diffraction investigations were carried out using the CuKα x-ray source at different 2° orientations (100–80°). Dynamic light scattering (Malvern Zetasizer Nano-ZS) was used to analyse the particle size of the synthesised Ag NPs.

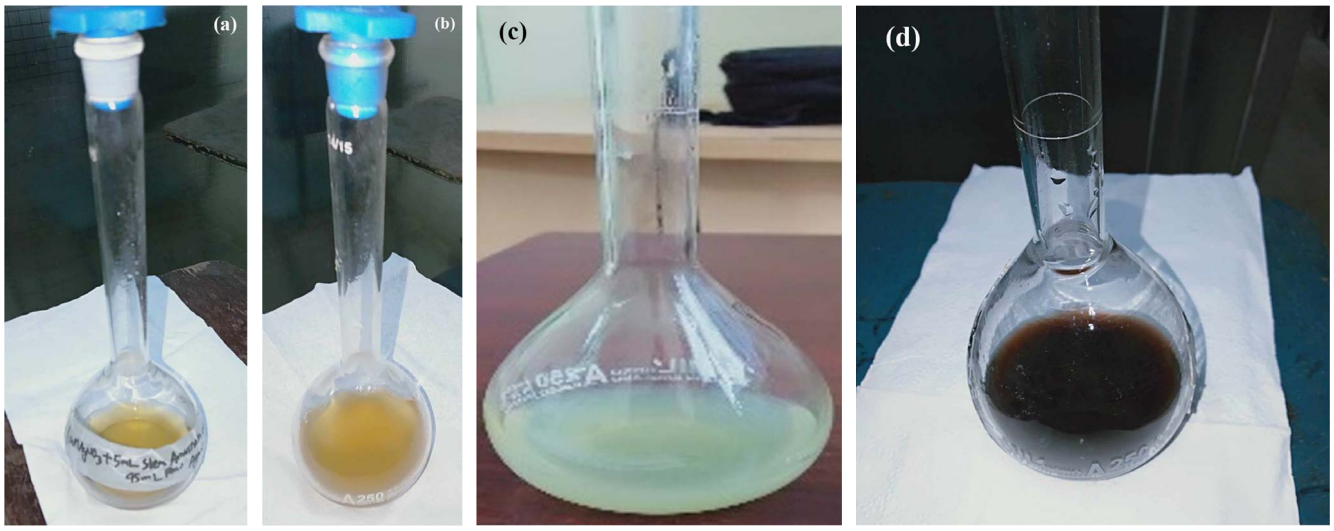

Figure 2. The visual alterations that occur as Ag NPs form.

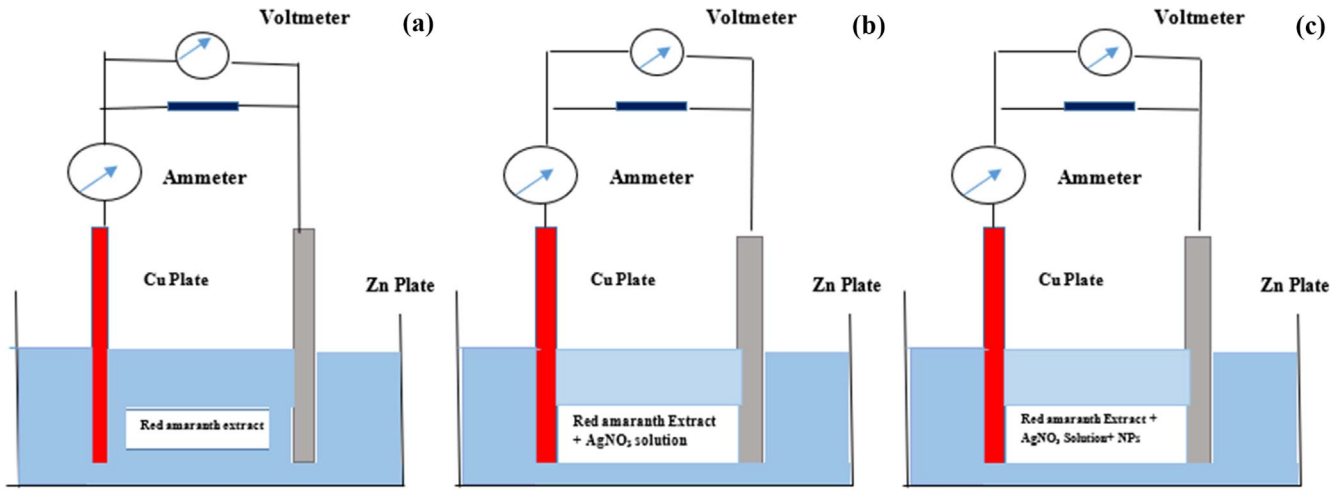

Figure 3. A test rig for putting the basic notion of zinc or copper-based red amaranth plant cells to the test.

For DLS measurements, powder Ag NPs were resuspended in distilled water and sonicated for 15–20 min to properly disperse the particles in water. Raman spectra were measured using a Bruker Raman spectrometer (model Senterra with laser excitation at 514 nm and laser power at 10 mW). Spectral data were collected using a 50-microscope objective (NA = 0:51) with integration time of 30 s. The silver nanoparticle samples were prepared by mixing 360 ml of colloidal solution with 40 ml of aqueous solutions of the probe molecule, resulting in a final Ag NP concentration of $1{:}0 \times 10^{-5}$ mol l^{-1}.

2.7. Operations of synopsis units for generating electricity

To further understand how silver nanoparticles work in the power-generating process, synopsis cells were treated with environmentally generated silver nanoparticles. Bio-electrochemical cells were used to electrolyse Ag NPs. Figure 4 illustrates how Ag NPs affect bio-electrochemical cells. Figure 4 depicts the voltage in the open circuit as a function of time. In figure 4(a), it is demonstrated that the voltage in an open circuit in a bending structure changes with time. It is demonstrated that the voltage in the open circuit rises steadily for up to 30 min, then quickly increases for up to 40 min, and finally decreases for up to 60 min. The current in a short circuit swings as the time period changes, as seen in figure 4(b). In a short circuit, the current first drops for 15 min, then rises quickly for 45 min, then drops again for 50 min, and finally rises for 60 min. In a short circuit, the current quickly decreases over a period of up to 50 min. The load current increases for up to 10 min, then increases quickly for up to 20 min, decreases gradually for up to 30 min, increases again for up to 40 min, and then abruptly decreases for up to 50 min, as shown in figure 4(c).

2.8. Bio-electrochemical cell chemical reaction

A bio-electrochemical cell is depicted (figure 5). In this case, Zn serves as a sacrificial element, acting as a cathode, while Cu serves as an anode.

Chemical reactions

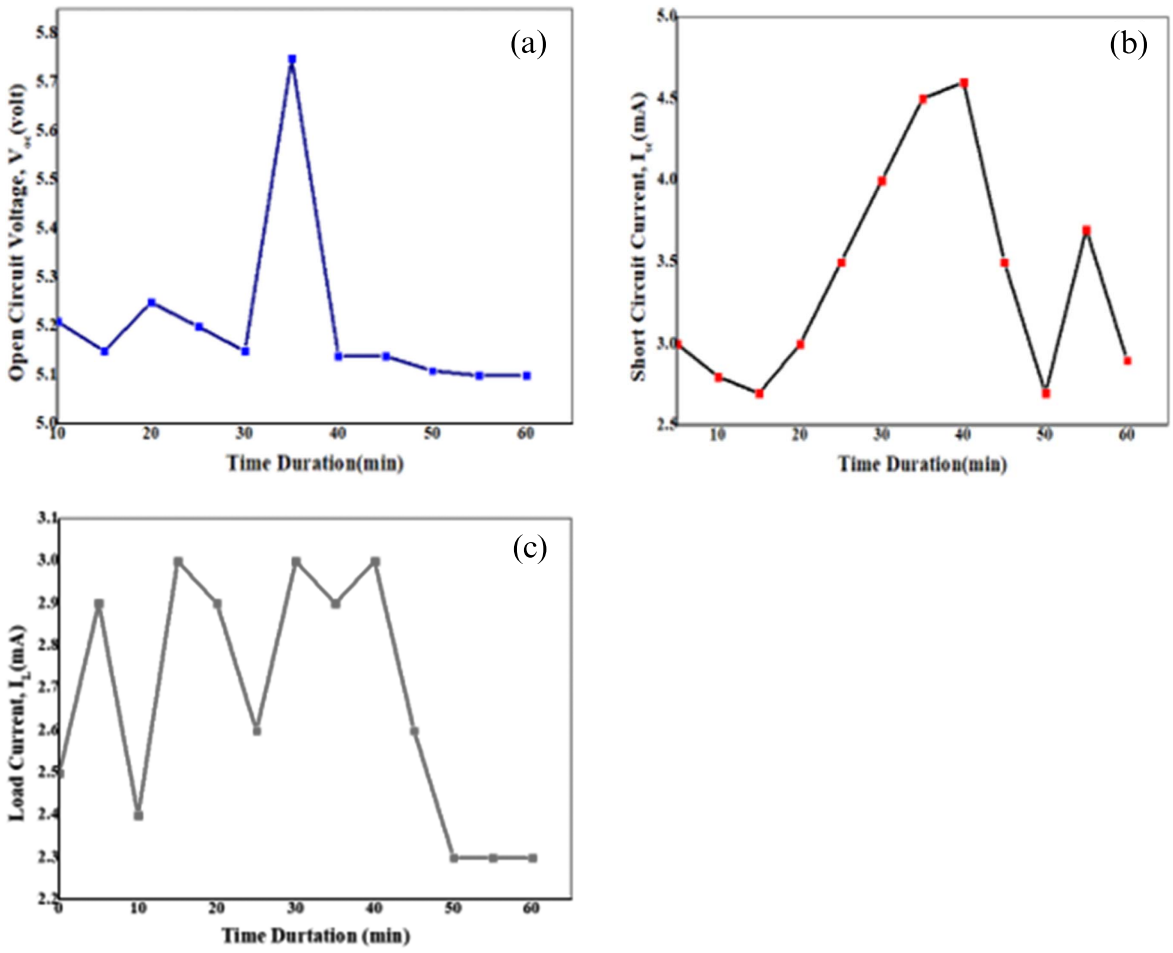

Figure 4. Red amaranth plant cells' electrical events (a) voltage in the open circuit with time duration, (b) current in the short circuit with time duration, and (c) load current with time duration.

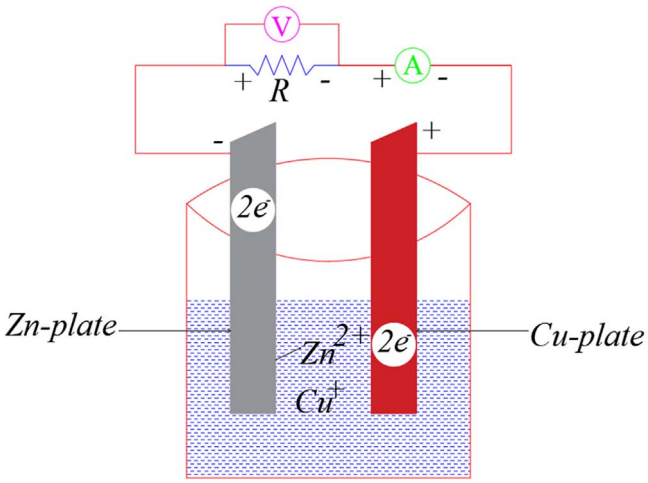

Figure 5. Bio-electrochemical cells.

(a) At zinc:

$$Zn = Zn^{2+} + 2e^{-}.$$

where, Zn^{2+} = Ionisation of the product in which Zn is called a sacrificial element.

(b) At copper:

$$Cu^{++} + 2e^{-} = Cu,$$

where, Cu^{2+} = Ion that reacts in which Cu is called the cathode. Adding:

$$Zn + Cu^{2+} = Zn^{2+}$$

where, Cu^{2+}= Ion that reacts and Zn^{2+} = Ionisation of the product.

(c) At zinc:

$$Zn = Zn^{2+} + 2e^{-},$$

where, Zn^{2+} = Ionisation of the product. At extract:

$$2H^{+} + 2e^{-} = H_2.$$

where, H^{+} = Ion that reacts. Adding:

$$Zn + 2H^{+} = Zn^{2+} + H_2.$$

where, H^{+} = Ion that reacts and Zn^{2+} = Ion that reacts. Total reaction:

$$Zn + Cu^{2+} + 2H^{+} = Zn^{2+} + Cu + H_2.$$

where, Cu^{2+} = Reactant ion, H^{+} = Ion that reacts and Zn^{2+} = Ion that reacts.

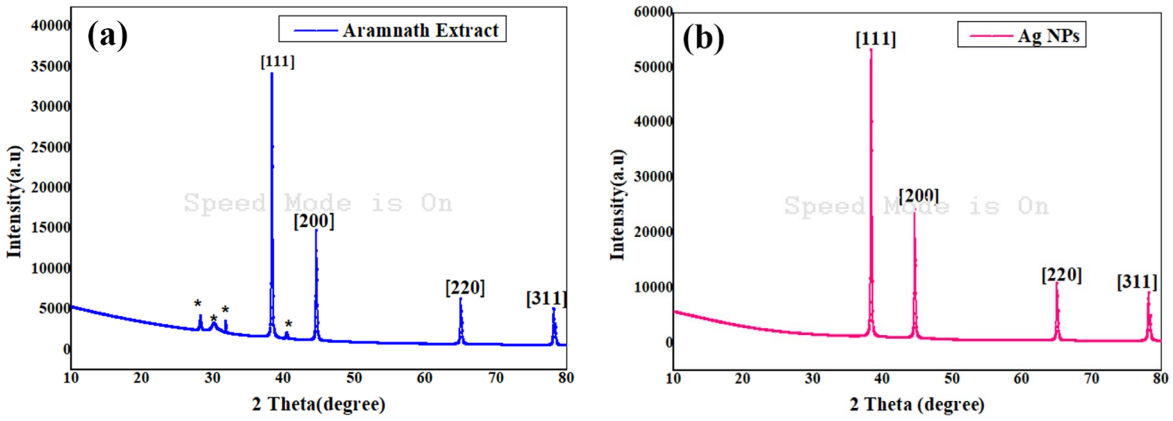

Figure 6. (a) Intensity versus 2 Theta for red amaranth extract, and (b) Intensity versus 2 Theta for synthesised Ag NPs for 5 ml red amaranth.

3. Result and discussions

3.1. Analysis using x-ray diffraction (XRD)

For 5 ml of red amaranth extract and produced Ag NPs, the XRD patterns for the extract and the NPs showed ten peaks each (figures 6(a) and (b)). The face-centered cubic structure of a typical silver crystal has four notable peaks with Bragg reflection values of 38.44°, 44.45°, 64.40°, and 78.50° at 2 theta values, respectively. These peaks correspond to the (111), (200), (220), and (311) crystallographic planes of face-centered cubic (FCC) silver with a lattice parameter of $a = 4.08$ Å which were in good agreement with reference to FCC structure from joint committee of powder diffraction standard (JCPDS) Card No-087–0720. These four distinct, wide peaks indicated that the Ag NPs had reduced in size and were extremely crystalline. The remaining small peaks indicate crystalline organic compounds that have been adsorbed on the surface of the Ag NPs. The found XRD pattern coincided with previous observations on plant-based synthesis [29]. By applying the Scherrer equation on the XRD pattern [29], the particle size can be calculated:

$$D = \frac{K\lambda}{\beta \cos\theta}. \tag{1}$$

where D is the mean size of crystallites (nm), K is the crystallite shape factor with a good approximation of 0.9, λ is the x-ray wavelength, β is the full width at half the maximum (FWHM) [30–32] in radian of the x-ray diffraction peak and θ is the Braggs' angle (deg.) [30]. The average crystal size of the green-produced Silver NPs is reported to be 16 nm. The significant peak [33] revealed that bioorganic chemicals and/or proteins were present in the NPs throughout the production process. Numerous publications received consistent findings, and the XRD pattern contained some notable highs (shown by a^*) [34–38].

Williamson–Hall analysis is a simplified integral breadth method employed for estimating crystal, crystallite size, and lattice strain, considering the peak width as a function of 2θ [39]. The crystallite size is not necessarily the same as particle size, since the crystallite size is assumed to be the size of a coherently diffracting domain. From equations (1) and (2), it is clear that the peak width from crystalline size varies as per the equation $1/\cos\theta$ and strain takes the equation $\tan\theta$. Assuming the particle size and the strain contributions to line broadening are independent of each other and both have Cauchy-like profile, the observed line breadth is taken as the following equations,

$$\beta = \frac{0.9\lambda}{D\cos\theta} + 4\varepsilon \tan\theta. \tag{2}$$

By rearranging equation (2), we get

$$\beta\cos\theta = \frac{0.9\lambda}{D} + 4\varepsilon \sin\theta. \tag{3}$$

Equation (3) is the Williamson–Hall equation, which assumes that the strain is uniform in all crystallographic directions. The crystallite size (D) and microstrain (ε) are calculated from the intercept ($k\lambda/D$) and slope of the line. The average crystal size of the green-produced silver NPs is reported to be 18.758 nm. Debye–Scherrer's and Williamson–Hall's analyses with the calculations are found to be closely matched.

3.2. UV–vis spectroscopy of biosynthesised Ag NPs

It came to light that the ultraviolet-visible spectrum analyser of a colloidal dispersion of silver nanoparticles was documented as a time function that used a crystal micropipette with water as regarded by studying the decrease of Ag ions in water solution of silver complicated throughout reactions with the components of red amaranth extract. The greatest absorption peak was seen at 428 nm, demonstrating that Ag+ reduction produces silver nanoparticle ions in the aqueous AgNO3 combination (figures 7(a), (b)).

Figure 7(a) displays the UV-visible spectra of a red amaranth extract (Pink line). From a total of 250 to 700-nanometer wavelengths, the pink line did not show any specific peak. During the synthesis process, adding PKL extract to the $AgNO_3$ solution caused the colour of the solution to change to darkish, indicating the formation of Ag^0 from the $AgNO_3$ solution. The oxidation of Ag required the plant's precise reductant [37]. The band emission of Ag NPs for 5 ml red amaranth, on the other hand, caused a strong peak to develop at about 428 nm as seen in figure 7(b).

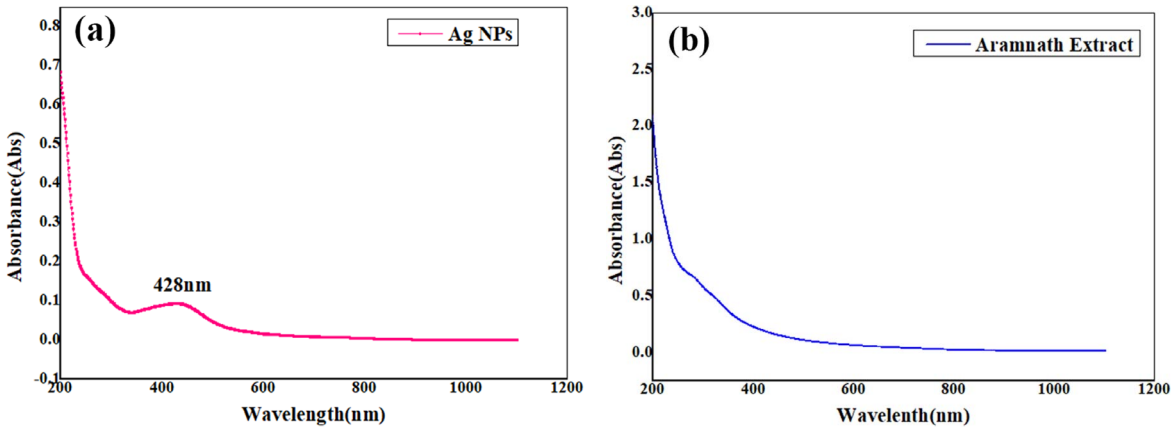

Figure 7. (a) UV-vis spectra for filtered red amaranth extract and (b) UV-vis spectra of Ag NPs for 5 ml red amaranth.

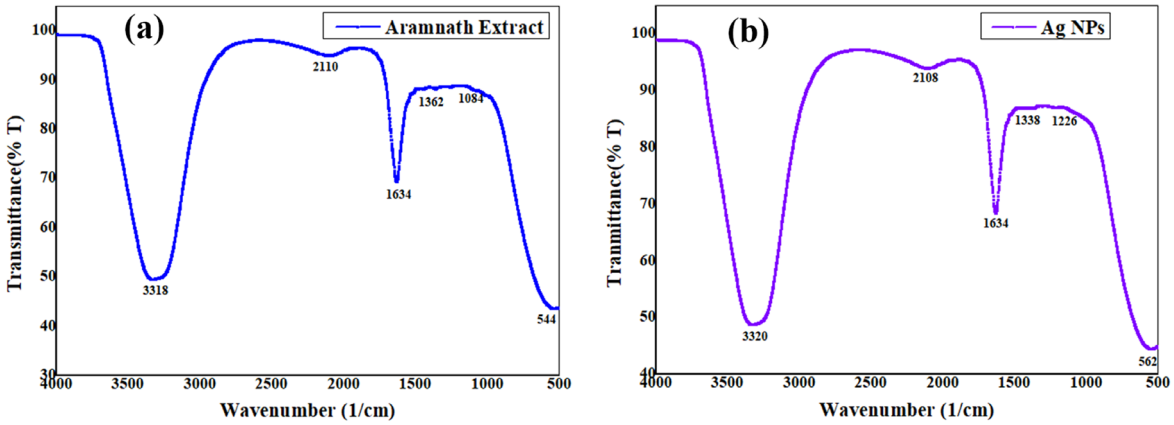

Figure 8. (a) FTIR of filtered red amaranth extract and (b) FTIR of red amaranth extract mediated Ag NPs for 5 ml.

3.3. FTIR analysis

Figure 8(a) shows the FTIR spectra of the red amaranth extract in order to identify potential bioactive silver ions produced from red amaranth that are responsible for the reduction and capping of the reduced Ag nanoparticles of red amaranth extract. Numerous peaks around 544 cm^{-1}, 1084 cm^{-1}, 1360 cm^{-1}, 1634 cm^{-1}, 2110 cm^{-1}, and 3318 cm^{-1} were seen in the spectrum. This finding revealed that Ag NPs mediated by red amaranth extract exhibited the largest peak, measuring 3318 cm^{-1}, with the O–H stretching vibration functional group. Alkyl aryl ether's CO bond's vibrational stretching may have contributed to the peak at about 544 cm^{-1}. The O–H bond's bending may be the cause of the peak at 1084 cm^{-1}. Furthermore, the stretching vibration of C=C caused the heights at around 1360 cm^{-1} to occur. A second high peak caused by the bending vibration of the C–C bond may be seen at about 2110 cm^{-1}. Furthermore, the O–H and N–H stretching may have contributed to the peak at wave number 3318 cm^{-1}.

The FTIR spectra of Ag NPs mediated by 5ml of red amaranth extract are shown in figure 8(b). Numerous peaks around 562 cm^{-1}, 1226 cm^{-1}, 1338 cm^{-1}, 1634 cm^{-1}, 2108 cm^{-1}, and 3320 cm^{-1} were seen in the spectrum. This finding revealed that the O–H stretching vibration functional group exhibited the greatest peak of 3320 cm^{-1} in red amaranth extract-mediated Ag NPs for 5 ml red amaranth. Alkyl aryl ether's CO bond's vibrational stretching may have contributed to the peak at about 562 cm^{-1}. The O–H bond's bending may be the cause of the peak at 1226 cm^{-1}. Furthermore, the stretching vibration of C=C caused the heights at around 1634 cm^{-1} to occur. The bending vibration of the CC bond results in another high peak that may be seen at about 2108 cm^{-1}. Furthermore, the O–H and N–H stretching may have contributed to the peak at wave number 3320 cm^{-1}.

3.4. DLS analysis

Figure 9 shows the size distribution profile of these biosynthesised silver nanoparticles of red amaranth extract-mediated Ag NPs for 5 ml. The Ag NPs were found to have a size distribution ranging from 20 to 113.6 nm. The DLS study is required to investigate the particle size in colloidal solution, and the curve obtained by scanning suspension of Ag nanoparticles indicates the average size (diameter) of the silver nanoparticles to be around 72.87 nm, which confirmed the good stability of Ag NPs [40].

3.5. Raman spectroscopy

The Raman spectra of Ag NPs, shown in figure 10, show the intensive peaks at 1977 cm^{-1}, 1884 cm^{-1}, and 1475 cm^{-1}.

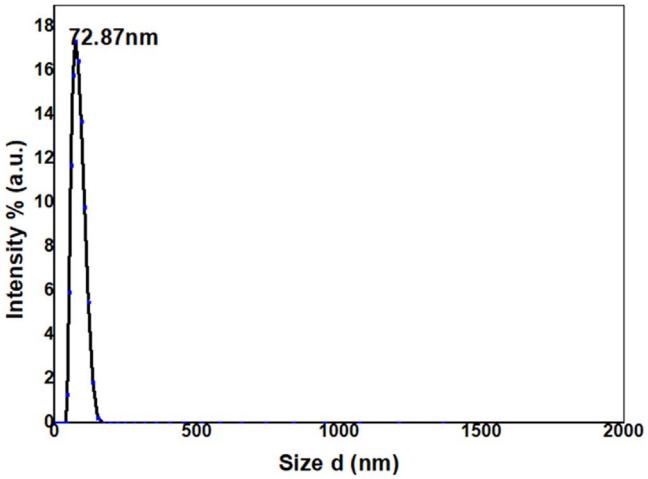

Figure 9. The size distribution profile of these biosynthesised silver nanoparticles of red amaranth extract-mediated Ag NPs for 5 ml.

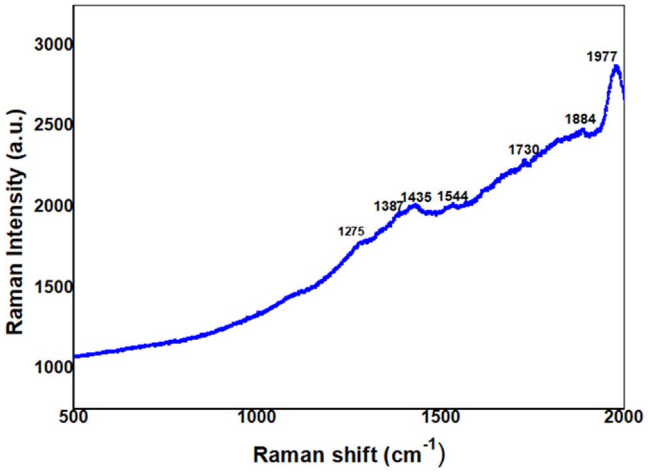

Figure 10. The Raman spectra of the Ag NPs of red amaranth extract-mediated Ag NPs for 5 ml.

These peaks indicate the interaction between the extract and $AgNO_3$ through the carboxylic and hydrophobic groups [41, 42]. The band located at 1275 cm^{-1} clearly indicates the presence of the silver lattice vibration models [43]. The bands situated at 1544 cm^{-1} and 1730 cm^{-1} indicate the presence of Ag NPs.

4. Conclusion

For the first time, Ag NPs are effectively synthesised in a quick, inexpensive, and environmentally friendly manner using red amaranth extract. Ag+ had been converted to Ag^0, as evidenced by the silver nanoparticles' highest ultraviolet-visible absorbance at 428 nm. Active functionalisation groups that are crucial to the reduction of silver nanoparticles were discovered in the FTIR spectra of Ag NPs. By using biological processes, spherical Ag nanoparticles with an average size of 16 nm were created. Notwithstanding the reality that several research on the environmentally friendly manufacturing of silver nanoparticles using diverse plant components has been published, the impact of Ag NPs on the lifespan of energy generation in organisms has been observed. Electrochemical cells are found for the first time in this experiment. The produced samples NPs increased the lifespan of red amaranth electrochemical cells in terms of energy generation. This might yield promising results that can be employed to characterise and understand the lifespan of electrochemical cell-mediated NP production for plant exclusives following extended exposure lifetime quality power generator device use. This revelation will spur further investigation into how organic cells create energy.

Acknowledgments

The authors are appreciative of Professor Dr A A Mamun for his kind assistance during this research at Jahangirnagar University in Savar, Bangladesh.

References

[1] Qian Y, Yu H, He D, Yang H, Wang W, Wan X and Wang L 2013 *Bioprocess. Biosyst. Eng.* **36** 1613–9
[2] Wang C, Kim Y J, Singh P, Mathiyalagan R, Jin Y and Yang D C 2015 *Artificial Cells, Nanomedicine, and Biotechnology* **44** 1127–32
[3] Mangala K J 2023 *Adv. Nat. Sci.: Nanosci. Nanotechnol.* **14** 035016
[4] Sundrarajan M, Bama K, Bhavani M, Jegatheeswaran S, Ambika S, Sangili A, Nithya P and Sumathi R 2017 *J. Photochem. Photobiol. B Biol.* **171** 117–24
[5] Tran Q H, Nguyen V Q and Le A-T 2013 *Adv. Nat. Sci.: Nanosci. Nanotechnol.* **4** 033001
[6] Salavati-Niasari M, ghanbari D and Davar F 2010 *J. Alloys Compd.* **492** 570–5
[7] Rivillas-Acevedo L and Soriano-Garcia M 2007 *J. Mex. Chem. Soc.* **51** 136–40
[8] Yousefi M, Gholamian F, Ghanbari D and Salavati-Niasari M 2011 *Polyhedron* **30** 1055–60
[9] Salavati-Niasari M, Hasanalian J and Najafian H 2004 *J. Mol. Catal. A: Chem.* **209** 209–14
[10] Aslany S, Tafvizi F and Naseh V 2020 *Mater. Today Commun.* **24** 101011
[11] Khan K A *et al* 2018 *Microsyst. Technol.* **26** 3161–72
[12] Khan K A, Mamun M A, Ibrahim M, Hasan M, Ohiduzzaman M, Obaydullah A K M, Wadud M A and Shajahan M 2019 *SN Applied Sciences* **1** 1335
[13] Khan K A, Ali M H, Mamun M A, Haque M M, Ullah A K M A, Khan M N I, Hassan L, Obaydullah A K M and Wadud M A 2022 *Microsyst. Technol.* **28** 823–32
[14] Vu X H, Duong T T T, Pham T T H, Trinh D K, Nguyen X H and Dang VS 2018 *Adv. Nat. Sci.: Nanosci. Nanotechnol.* **9** 025019
[15] Salavati-Nasasari M 2004 *J. Mol. Catal. A: Chem.* **217** 87–92
[16] Salavati- Nasasari M and Amiri A 2005 *Appl. Catal.*A **290** 46–53
[17] Ashok Kumar B S, Lakshman K, Jayaveera K N, Sheshadrishekar D, Narayan Swamy V B, Khan S and Velumurga C 2011 *Oman Med. J.* **26** 166–70
[18] Girija K, Lakshman K, Chandrika U, Ghosh S S and Divya T 2011 *Asian Pac. J. Trop. Biomed.* **1** 133–8

[19] Venshutonis P R and Kraujalis P 2013 *A. J. Food Sci.* **12** 381–412
[20] Kumar B, Smita K, Seqqat R, Benalcazar K, Grijalva M and Cumbal L 2016 *J. Photochem. Photobiol. B Biol.* **159** 8–13
[21] Garibo D *et al* 2020 *Sci. Rep.* **10** 12805
[22] Chavan R R, Bhinge S D, Bhutkar M A, Randive D S, Wadkar G H, Todkar S S and Urade M N 2020 *Mater. Today Commun.* **24** 101320
[23] Jebril S, Khanfir Ben Jenana R and Dridi C 2020 *Mater. Chem. Phys.* **248** 122898
[24] Panahi A, Monsef R, Imran M K, Mahdi A A, Kadhim Ruhaima A A and Salavati-Niasari M 2023 *Int. J. Hydrogen Energy* **48** 3916–30
[25] Narayanan K B and Sakthivel N 2008 *Mater. Lett.* **62** 4588–90
[26] Paul B, Khan K A and Paul M 2022 *Micro and Nanoelectronics Devices, Circuits and Systems* **904** 455–65
[27] Hossain M A, Paul B, Khan K A, Paul M, Mamun M A and Quayum M E 2022 *Mater. Chem. Phys.* **282** 125943
[28] Shankar S, Rai A, Ankamwar B, Singh A, Ahmad A and Sastry M 2004 *Nat. Mater.* **3** 482–8
[29] Jayaprakash N, Vijaya J J, Kaviyarasu K, Kombaiah K, Kennedy L J, Ramalingam R J, Munusamy M A and Al-Lohedan H A 2017 *J. Photochem. Photobiol. B Biol.* **169** 178–85
[30] Leela A and Vivekanandan M 2008 *African J. of Biotechnol.* **7** 31662- 33165
[31] Shankar S S, Rai A, Ahmad A and Sastry M 2004 *J. Colloid Interface Sci.* **275** 496–502
[32] Hasim H, Rao P V, Sekhar A C, Muthuraju S, Asari M A and Sirajudeen K N S 2020 *Adv. Nat. Sci.: Nanosci. Nanotechnol.* **11** 025010
[33] Zamiri R, Zakaria A, Husin M S, Wahab J A and Nazarpour F K 2011 *Int. J. Nanomed.* **6** 2221–4
[34] Kalpana D and Lee Y S 2013 *Enzym. Microb. Technol.* **52** 151–6
[35] Aziz N, Faraz M, Pandey R, Shakir M, Fatma T, Varma A, Barman I and Prasad R 2015 *Langmuir* **31** 11605–12
[36] Suvith V S and Philip D 2014 *Spectrochim. Acta Mol. Biomol. Spectrosc.* **118** 526–32
[37] Hamedi S, Shojaosadati S A and Mohammadi A 2017 *J. Photochem. Photobiol. B Biol.* **167** 36–44
[38] Anandalakshmi K, Venugobal J and Ramasamy V 2016 *Appl. Nanosci.* **6** 399–408
[39] Sundeep D, Krishna A G, Ravikumar R V S S N, Kumar T V, Ephraim S D and Pavan Y L 2016 *Int. Nano Lett.* **6** 119
[40] Patil S V, Borase H P, Patil C D and Salunke B K 2012 *Appl. Biochem. Biotechnol.* **167** 776–90
[41] Salari Z, Danafar F, Dabaghi S and Ataei S A 2016 *Journal of Saudi Chemical Society* **20** 459–64
[42] Ali M, Kim B, Belfield K D, Norman D, Brennan M and Ali G S 2016 *Materials Science and Engineering*C **58** 359–65
[43] Venugopal K, Ahmad H, Manikandan E, Thanigai Arul K, Kavitha K, Moodley M K, Rajagopal K, Balabhaskar R and Bhaskar M 2017 *J. Photochem. Photobiol.*B **173** 99–107